

Atomistic simulations of long-range strain and spatial asymmetry effects in multimillion-atom single and double quantum dot nanostructures

Gerhard Klimeck^{1,2}, Marek Korkusinski¹, Haiying Xu¹, Seungwon Lee²,
Sebastien Goasguen¹, and Faisal Saied¹

¹Network for Computational Nanotechnology, School of Electrical and Computer Engineering, Purdue University,
465 Northwestern Avenue, West Lafayette IN 47907, USA

²Jet Propulsion Laboratory, California Institute of Technology, Pasadena CA 91109, USA

E-mail: gekco@purdue.edu

Abstract – The Nanoelectronic Modeling Tool NEMO-3D is a simulator providing quantitative estimates for the strain distribution and the single-particle electronic structure of semiconductor nanodevices, such as self-assembled quantum dots, quantum wells and wires. Both strain and electronic structure are computed using semi-empirical nearest-neighbor tight-binding schemes implemented on the atomistic level. The software tool is parallelized using MPI, which makes it possible to treat multimillion-atom systems. This work reports on application of the NEMO-3D tool to single and coupled quantum dot nanostructures. The spatial extent and directionality of the strain field produced by a single InAs quantum dot embedded in the GaAs barrier material is explored. In the multidot systems, the electron and hole states are computed as a function of the interdot distance for vertically coupled double-dot molecules.

I. INTRODUCTION

Quantum dots (QDs) are nanostructures which confine the motion of charge carriers in all spatial directions [1]. This confinement is strong enough for the quantum properties of carriers to dominate the device performance and characteristics. Recent progress in nanofabrication techniques resulted in the development of several types of QDs, exploiting different aspects of this quantum behavior [2,3]. This work focuses on self-assembled QDs (SADs) in the InAs/GaAs material system. These structures are capable of trapping both electrons and holes [3], which can interact optically. For this reason the SADs are of interest in quantum optics, since they can be used as emitters and detectors of infrared radiation [4], optical memories [3] and single-photon sources [5]. Arrays of quantum-mechanically coupled SADs are also used as optically active media in high efficiency, room-temperature lasers [6].

The SAD devices are composed of small (typical dimensions of order of tens of nanometers) crystals of the quantum well material (e.g., InAs) embedded in a quantum barrier (e.g., GaAs). Due to this small device size the atomistic granularity of the underlying crystal lattice cannot be neglected. Also, the self-assembly process of the QD systems is driven by the strain, resulting from the mismatch of lattice constants of the constituent materials [7]. The resulting strain field has a long-distance character and dramatically influences the energy diagram of the system [8]. These properties constrain the design of the simulator software – it has to model the relatively short-distance quantum behavior of charge carriers (confined inside the

QD) on equal footing with the long-distance, essentially classical strain effects. The Nanoelectronic Modeling Tool NEMO-3D meets these objectives by employing semi-empirical atomistic tight-binding models both for the strain and electronic structure calculations. Since the systems under consideration can contain tens of millions of atoms, this simulator is very demanding computationally. For this reason NEMO-3D was parallelized using MPI protocols and ported to several HPC platforms. This presentation describes the design and performance characteristics of NEMO-3D and summarizes the simulation results for single QDs as well as vertically coupled QD systems.

II. THE SYSTEM

Here NEMO-3D is used to investigate the electronic properties of InAs QD systems embedded in a GaAs barrier material. A typical layout of a single-dot system is presented in Figure 1. The base diameter of the dome-shaped QD is 18.09 nm, and its height is 1.7 nm. The dot is placed on a 0.6-nm-thick wetting layer. The system properties are computed on a domain containing the QD and a certain amount of the barrier surrounding the dot. However, the size of the domain depends on the property being addressed: in the computations of strain the domain is large due to the long-distance character of the strain field. In the electronic part, on the other hand, only the confined electronic states are targeted. Since their wave functions decay exponentially in the barrier, it is typically sufficient to consider a smaller domain. Also, a variety of boundary conditions can be applied to the domain walls, reflecting various possible environments of the system

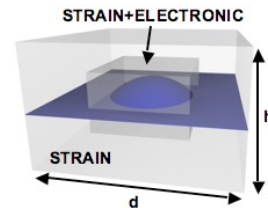


Fig. 1. A schematic view of a single QD nanostructure, composed of a dome-shaped InAs QD placed on a wetting layer. The strain is computed for atoms contained the larger domain, while the electronic structure calculations can be restricted to the smaller computational box.

III. THE SIMULATOR

NEMO-3D is a nanostructure modeling tool designed to provide *quantitative* predictions of the electronic structure of nanodevices [9, 10]. It employs semi-empirical tight binding models, which resolve the structure of the

treated system in atomistic detail. The calculation process consists of two parts: 1) strain distribution and 2) electron and hole eigenenergies and eigenstates.

The strain distribution is calculated in the frame of the valence force field model [8], in which the total elastic energy is a functional of the atomic displacements. A conjugate gradient algorithm is used to find the displacement field minimizing this functional. For a sample containing N atoms, each atom is assigned three numbers representing its spatial coordinates. The nonlinear CG algorithm used here requires that nine vectors of length of $3N$ be simultaneously stored in the memory; eight double precision vectors are divided among the P CPUs assigned to the task, while one single precision vector exists in full on each CPU for computational convenience. All terms of the energy functional are computed on the fly.

The electronic structure part employs the $sp^3d^5s^*$ first-nearest-neighbor tight-binding model. In this approach, each atom is assigned 20 localized orbitals treated as the orthonormal basis set. The Hamiltonian matrix is built in this basis. The empirical parameters had been fit with a genetic algorithm to represent experimental bulk properties under various strain conditions. Since the model allows for the nearest-neighbor coupling only, the resulting Hamiltonian is very sparse which is taken into account in the storage scheme. For the zincblende materials, the Hamiltonian contains at most 100 nonzero elements per row, irrespective of the number N . The memory allocation is also distributed among the computational nodes by dividing the sample into vertical slices, each slice assigned to one CPU. Due to the nearest-neighbor character of the model, only the CPUs assigned to adjacent slices need to communicate during the computation. The eigenvalues and eigenvectors of the Hamiltonian are found using the Lanczos algorithm.

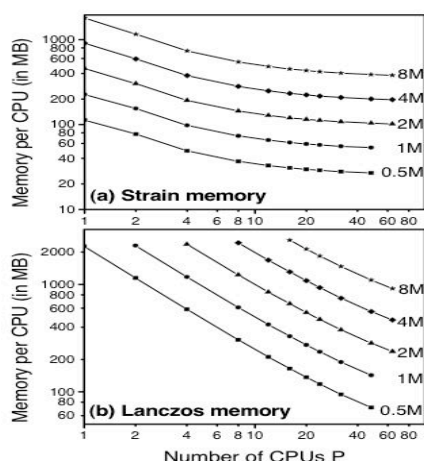


Fig. 2. Memory per CPU required for the computations of strain (a) and electronic structure (b) as a function of the number of CPUs P for systems containing different atom numbers.

Figure 2 shows the memory per CPU allocated in the strain (a) and electronic structure calculations (b) as a function of the number of CPUs assigned to the task for systems of different sizes. The memory requirements of NEMO-3D scale approximately linearly both with the

number of atoms and the number of CPUs P . The only exception occurs for strain at large numbers P , for which a saturation effect in memory scaling is seen. This effect is due to the existence of several unparallelized data structures, initialized on each CPU. In the electronic computations these structures exist as well, but their effect on memory allocation is smaller due to the much larger overall memory usage in this part. The maximal tractable system size depends on the amount of available memory per CPU: for a 2 GB/CPU system, it is possible to compute strain for 35.21 (39.17) million atoms, and the electronic structure for 6.18 (10.87) million atoms on 16 (32) CPUs, respectively. For a system with 11.5 GB/CPU, these numbers are 202.95 (225.74) million atoms for strain, and 35.59 (62.65) million atoms for electronics, respectively.

NEMO-3D has been ported to and tested on several HPC platforms. Figure 3 shows the time required for 100 strain iterations (a) and 400 Lanczos iterations (b) for a one-million-atom sample on five platforms: (i) a 64-bit IBM p690 shared memory machine with Power 4 1.7 GHz CPUs, (ii) an Apple G5 Power PC with 2GHz CPUs, (iii) an Apple G4 Power PC with 1GHz CPUs, (iv) an Intel Pentium 4 cluster with 3.06 GHz CPUs, and (v) an Intel Xeon cluster with 3.06 GHz CPUs. Systems (ii) – (iv) were equipped with Gigabit Ethernet, while the system (v) employed the Infiniband network. Overall, the performance on all platforms seems to scale reasonably well with the number of CPUs, although the cluster computer data in Fig. 3(a) appear to exhibit fluctuations, which we associate with network noise. This is due to the fact that the strain calculations are more communication-heavy than the electronics part, and so the performance is more sensitive to the type and state of the network. The electronics performance (Fig. 3(b)) is nearly linear with the number of CPUs. Out of the HPC platforms considered, the IBM system exhibited the best and most stable performance, while the clusters perform extremely well as low cost competitors.

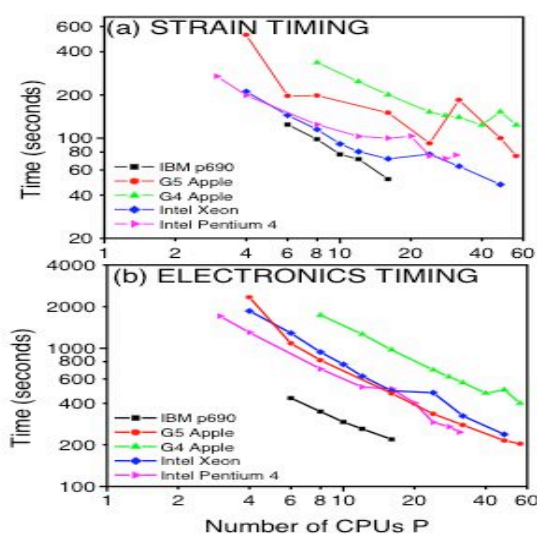


Fig. 3. Timing graphs of 100 CG strain iterations (a) and 400 Lanczos iterations (b) for a system of 1 million atoms on different HPC platforms (see text for details).

IV. A SINGLE SELF-ASSEMBLED DOT

Extraction of targeted eigenstates. Since the tight-binding model used in the electronic calculations involves 20 base orbitals per atom, the corresponding Hamiltonian matrix is of order of $20N$, where the number of atoms N can be of order of tens of millions. Only several of the corresponding eigenstates, with energies falling in the middle of the spectrum, are physically relevant. The NEMO-3D Lanczos solver is able to extract those targeted and unique eigenstates. To demonstrate that, Fig. 4 shows horizontal cross-sections of the ground and first excited electronic orbitals of the same SAD embedded in a computational domain composed of 300 000 (left) and 21 million (right) atoms. As can be seen, states of correct symmetry can be reliably extracted from the Hamiltonian spectrum even for the largest computational domains.

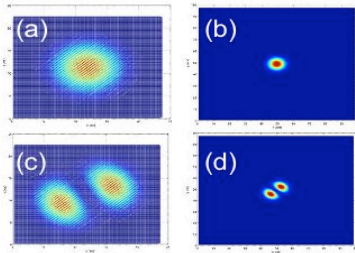


Fig. 4. Horizontal cross-sections of the ground (top) and first excited (bottom) electronic orbitals for the same dome-shaped SAD embedded in a computational box with 300 000 (left) and 21 million (right) atoms.

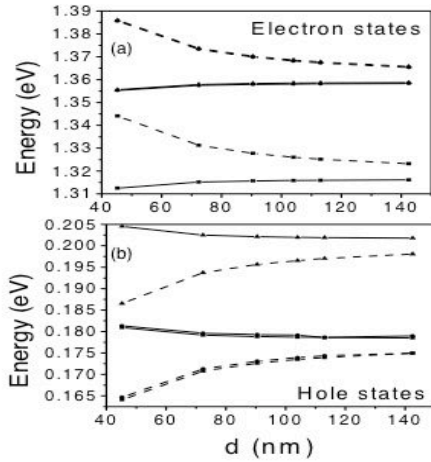


Fig. 5. Energies of the ground and first two excited states of an electron (a) and a hole (b) confined in the SAD as a function of the lateral size d of the strain domain. The domain aspect ratio $d/h=2$, and mixed (solid lines) and fixed (dashed lines) boundary conditions are applied to its walls.

Extent of the strain field. The second study examines the sensitivity of the confined electron and hole states to the extent of the strain domain and the boundary conditions employed on its walls. The SAD is unchanged, as is the electronic domain (it contains 2 million atoms), but the size of the strain domain is increased until it contains 64 million atoms. In this process, the aspect ratio d/h (cf. Fig. 1) is fixed to 2. Moreover, the computations are performed

under two sets of boundary conditions (BCs) applied to the strain domain: fixed, in which the atoms on the walls are fixed to the bulk GaAs positions, and mixed, in which the bottom wall is fixed, the top wall is free, and periodic BCs are applied to the side walls. The second set of BCs models an array of strain-coupled SADs grown on a thick substrate (hence the fixed bottom) and a finite cap layer (hence the free top surface). The interdot distances considered in this study are too large for the quantum-mechanical coupling of SADs to occur, and so fixed BCs are applied to the electronic domain. Figure 5 shows the energies of the ground and two first excited states of a carrier confined in the SAD as a function of the size d . As can be seen, the single-particle energies are very sensitive to the size of the strain domain, and do not converge even for $d=140$ nm – an indication of the long-range character of the strain field. Also, the rate of convergence depends on the BCs: for mixed BCs the sensitivity is weaker, since the strain can effectively relax through the free top surface of the sample. Mixed BCs represent physical reality for any d , and will be used in the remainder of this work.

Directionality of the strain field. The rate of convergence of the single-particle energies with the size of the strain domain also depends on the domain shape. Figure 6 shows the eigenenergies as a function of the dimension d computed for the aspect ratio $d/h=2$ and 0.5. The energies converge much faster in the latter case, in which the strain domain is pillar-shaped. This indicates that the strain field generated by the SAD has a dominant vertical component. This component is responsible for the vertical self-alignment of SADs belonging to adjacent vertical layers [11].

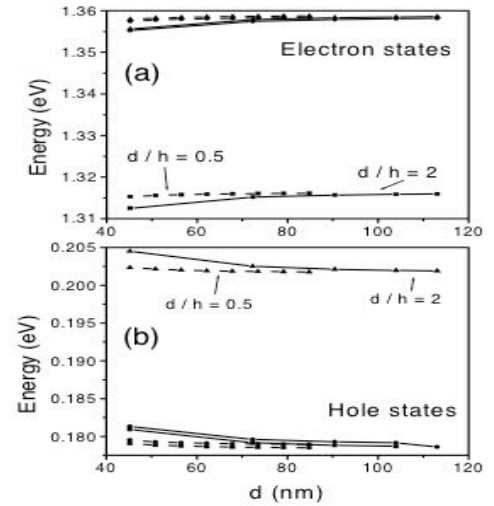


Fig. 6. Electron (a) and hole (b) energy levels as a function of the lateral dimension d of the strain domain for aspect ratios $d/h=2$ (solid lines) and 0.5 (dashed lines).

V. VERTICALLY COUPLED SAD MOLECULE

The last study of this work treats one of such self-aligned structures, schematically shown in Fig. 7. It is composed of two SADs sharing the vertical axis of rotational symmetry. The SADs are truncated domes, well approximated by disks; their heights are 2.83 nm each, and their radii $R_1=6.5$ nm and $R_2=6.96$ nm (these dimensions

correspond to those reported in Ref. [11]). Figure 8 shows the six lowest electron and hole energies computed as a function of the distance D between dot layers. The electron levels exhibit the behavior characteristic for the bonding and antibonding quantum-molecular orbitals [12]. The hole orbitals, on the other hand, appear to be confined to single SADs rather than shared between SADs, which is clearly seen in the distributions of the respective probability densities (not shown here).

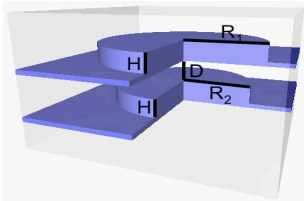


Fig. 7. A schematic view of the vertically coupled double-SAD molecule built of two truncated dome-shaped QDs.

To identify the reason of this difference between electron and hole states, similar calculations were performed for the system without strain, and also for identical dots with $R_1=R_2=6.5$ nm with and without strain. The energies of the two lowest electron and hole orbitals as a function of D are shown in Fig. 9. Without strain, the molecular behavior is seen for electrons and holes even when the disks are not identical. At large D , the orbitals are those of isolated QDs, which is why the corresponding energies are nondegenerate for nonidentical QDs. The inclusion of strain is responsible for the qualitative change in the character of the hole states: they become localized on single QDs even when the disks are identical.

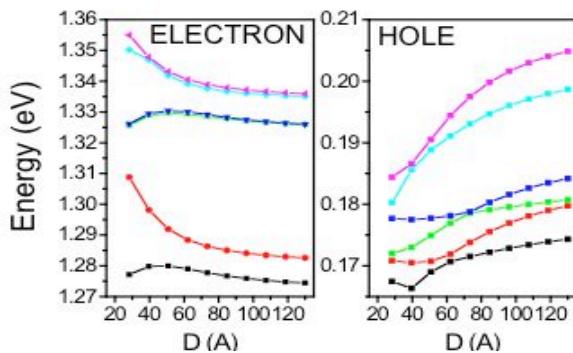


Fig. 8. Energies of the six lowest electron (left) and hole (right) states as a function of the distance D in a quantum molecule with $R_1 \neq R_2$.

CONCLUSIONS

The NEMO 3-D capability to extract meaningful, targeted eigenstates out of systems containing 21 million atoms is demonstrated. NEMO 3-D enables the simulation of realistically sized systems of vertically stacked quantum dots. The importance to consider inhomogeneous strain distributions and spatial asymmetry of typically vertically coupled quantum dots is demonstrated. The formation of bonding and anti-bonding states as a function of quantum dot separation is shown. No molecular hole states are observed in the realistic system, while the introduction of simplifications such as “no strain” results in molecular states.

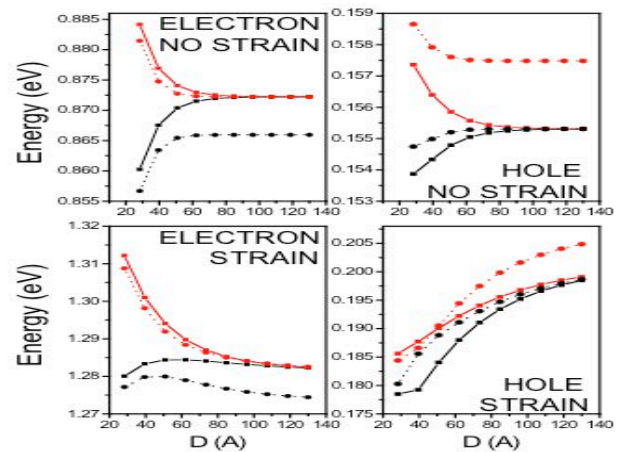


Fig. 9. Energies of the two lowest electron (left) and hole (right) states as a function of the distance D for a quantum molecule with $R_1=R_2$ (solid lines) and $R_1 \neq R_2$ (dotted lines) for a system without strain (top) and with strain (bottom).

ACKNOWLEDGMENTS

The work described in this publication was carried out in part at the Jet Propulsion Laboratory, California Institute of Technology under a contract with the National Aeronautics and Space Administration. Funding at Purdue was provided by NSF under Grant No. EEC-0228390 and by the Indiana 21st Century Fund. At JPL funding was provided under grants from ONR, ARDA, and JPL.

REFERENCES

- [1] For reviews and references see, e.g., L. Jacak, P. Hawrylak, and A. Wojs, “Quantum dots”, Springer-Verlag, Berlin, 1998; D. Bimberg, M. Grundmann, and N. N. Ledentsov, “Quantum Dot Heterostructures”, Wiley, London, 1999.
- [2] “Electron Transport in Quantum Dots”, J. P. Bird (Editor), Springer-Verlag, Berlin, 2003.
- [3] “Single Quantum Dots: Fundamentals, Applications and New Concepts”, P. Michler (Editor), Topics in Applied Physics, Springer, Berlin, 2003.
- [4] B. Aslan, H. C. Liu, M. Korkusinski, S.-J. Cheng, and P. Hawrylak, *Appl. Phys. Lett.* **82**, 630 (2003).
- [5] P. Michler *et al.*, *Science* **290**, 2282 (2000); E. Moreau *et al.*, *Phys. Rev. Lett.* **87**, 183601 (2001).
- [6] “Quantum Dot Lasers”, A. E. Zhokov *et al.* (Editors), Series on Semiconductor Science and Technology, Oxford University Press, Oxford, 2003.
- [7] P.M. Petroff and S.P. DenBaars, *Superlatt. Microstruct.* **15**, 15 (1994).
- [8] M. Tadic *et al.*, *J. Appl. Phys.* **92**, 5819 (2002) and references therein.
- [9] G. Klimeck *et al.*, *Computer Modeling in Engineering and Science* **3**, 601 (2002).
- [10] F. Oyafuso *et al.*, *J. Comput. Electronics* **1**, 317 (2002).
- [11] Z. R. Wasilewski, *et al.*, *J. Cryst. Growth* **201**, 1131 (1999); S. Fafard *et al.*, *Appl. Phys. Lett.* **75**, 986 (1999).
- [12] M. Korkusinski *et al.*, *Physica E* **13**, 610 (2002); M. Bayer *et al.*, *Science* **291**, 451 (2001).